



## Research paper

## Luminescence dating and associated analyses in transition landscapes of the Alto Ribatejo, central Portugal



C.I. Burbidge<sup>a,e,\*</sup>, M.J. Trindade<sup>a,e</sup>, M.I. Dias<sup>a,e</sup>, L. Oosterbeek<sup>b,d</sup>, C. Scarre<sup>c</sup>, P. Rosina<sup>b,d</sup>, A. Cruz<sup>b</sup>, S. Cura<sup>d</sup>, P. Cura<sup>d</sup>, L. Caron<sup>b</sup>, M.I. Prudêncio<sup>a,e</sup>, G.J.O. Cardoso<sup>a</sup>, D. Franco<sup>a</sup>, R. Marques<sup>a,e</sup>, H. Gomes<sup>d</sup>

<sup>a</sup> C<sup>2</sup>TN, Campus Tecnológico e Nuclear, Instituto Superior Técnico, Universidade de Lisboa, EN 10, km 139,7, 2695-066 Bobadela LRS, Portugal

<sup>b</sup> Instituto Politécnico de Tomar, Campus Tomar, Quinta do Contador – Estrada da Serra, 2300-313 Tomar, Portugal

<sup>c</sup> Durham University, Department of Archaeology, South Road, Durham DH1 3LE, UK

<sup>d</sup> Instituto Terra e Memória, Largo Infante D. Henrique, 6120-750 Mação, Portugal

<sup>e</sup> GeoBioTec, Universidade de Aveiro, Campus Universitário de Santiago, 3810-193 Aveiro, Portugal

## ARTICLE INFO

## Article history:

Received 9 February 2013

Received in revised form

6 November 2013

Accepted 7 November 2013

Available online 18 November 2013

## Keywords:

OSL

INAA

Gamma-spectrometry

XRD

Agro-pastoralism

Megalithic

Landscape-activation

Holocene

## ABSTRACT

Artefacts and regolith (soils, sediments, colluvia, etc.) from passage tombs, pit fills, stone scatter and clay structures, related to the transition to agro-pastoralism in the Alto Ribatejo, were analysed by optically stimulated luminescence, neutron activation analysis, field and high-resolution gamma spectrometry, and X-ray diffraction. Indications of anthropogenic, autogenic, and allogenic site formation and diagenetic processes, including radionuclide exchange, were applied to interpret 28 date estimates from the 9th to 1st millennia BC. Results from regolith samples relate to different phases of landscape activation and stability from the late 6th millennium BC to the Roman conquest. However, simple archaeological questions were best answered using heated materials, where present. Different chronological phases were often represented by different sample types in sites with multi-phase stratigraphies, indicating the importance of parallel analyses. Results from a fire pit coincide with the first indications of clearance in the regional pollen record (late 9th millennium BC): these features appear promising to map early Holocene human presence in the Alto Ribatejo landscape.

© 2013 Elsevier B.V. All rights reserved.

## 1. Introduction

The performance and interpretation of thermally or optically stimulated luminescence (TSL, OSL) dating analyses are interdependent with the archaeological, geochemical, mineralogical, geomorphological, and hydrological context of the samples being analysed (Aitken, 1985). In the dating of re-deposited mineral grains by OSL, the event of interest is their last exposure to light during transport. Chrono-stratigraphic points of view provided by the luminescence dating of heated artefacts include the direct dating of structures or typologies (e.g. Whittle and Arnaud, 1975), and the dating of undiagnostic sherds as geoarchaeological

artefacts (e.g. Deckers et al., 2005). Questions of residuality, association, geometry, and alteration to be asked of the regolith are different to those of the heated artefact, so their parallel measurement using the same method can lend security to the dating of a context, while differences between results may be effectively applied to understand complex site-formation histories.

The presence of mineral fractions, and their luminescence behaviour, depends on geological source material, and the production technology of archaeological artefacts. Archaeological contexts are often subject to complex formation mechanisms and diagenetic changes. These may produce patterns of residuality in luminescence signals or samples (from transported grains or artefacts, Barnett, 2000; Burbidge et al., 2007), complex dosimetric geometries (Aitken, 1985), and changes in the geometry and radioisotope contents of a sample or its surroundings through time (Guibert et al., 2009; Zacharias et al., 2007). Instrumental neutron activation analysis (INAA) and X-ray diffraction (XRD) provide parent element concentrations and mineral concentrations, and are

\* Corresponding author. C<sup>2</sup>TN, Campus Tecnológico e Nuclear, Instituto Superior Técnico, Universidade de Lisboa, EN 10, km 139,7, 2695-066 Bobadela LRS, Portugal.  
E-mail address: [christoph@ctn.ist.utl.pt](mailto:christoph@ctn.ist.utl.pt) (C.I. Burbidge).

**Table 1**  
Holocene environmental, climatic, and geomorphic context, summarized from van der Knaap and van Leeuwen (1995), Vis et al. (2010), Abrantes et al. (2005), and van der Schriek (2004). P = Palaeolithic, EP = Epipalaeolithic, M = Mesolithic, N = Neolithic, C = Chalcolithic, BA = Bronze Age, IA = Iron Age, R = Roman, Med = Mediaeval, PM = Post Mediaeval. 235 <sup>14</sup>C, 27 TSL/OSL and 7 U-series results from ascribed contexts, plus 'Me' from otherwise unassigned megalithic contexts were binned in each timeline division simply using each central estimate (from the database of Cardoso et al., 2012). The area 9–5 °W, 39–40 °N, was chosen to include Spanish Extremadura, the shell middens of the lower Tejo and Portuguese Extremadura, and the Alto Ribatejo, Uncalibrated <sup>14</sup>C data were converted using Reimer et al. (2009), other data are as reported. Problems of method, interpretation/association, and residual/intrusive materials/signals etc. produce tails in the distributions of dates for a given period, and of periods for a given date.

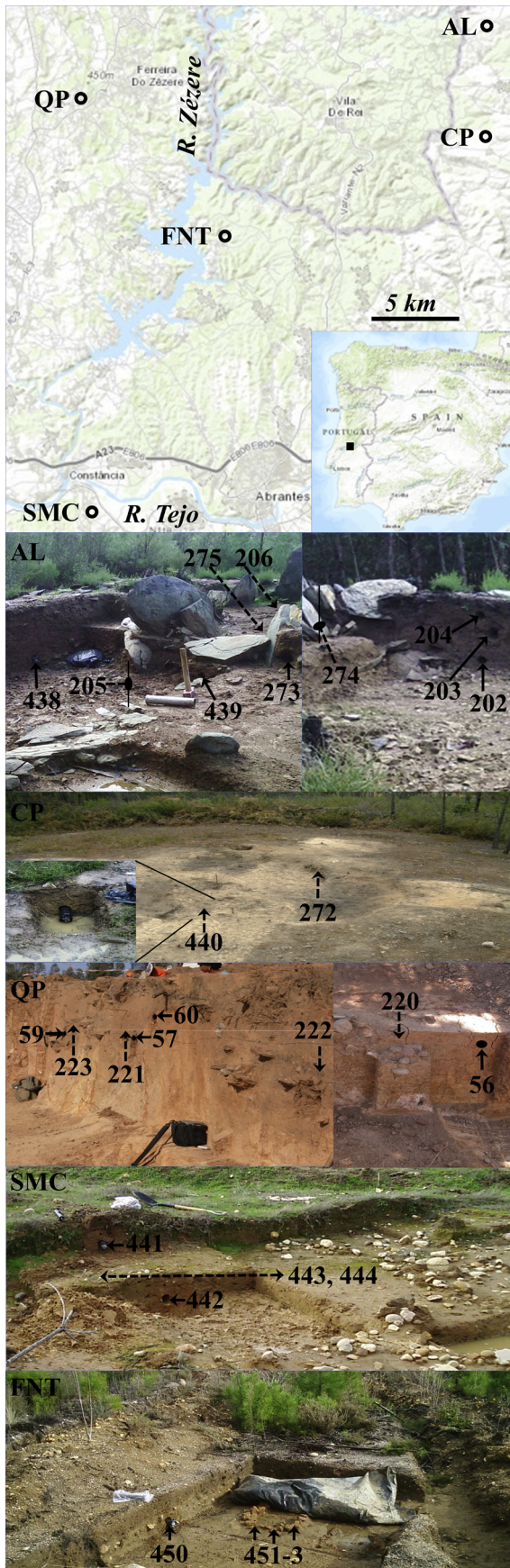
Timeline (BC/AD)	Vegetation	Climate	Sedimentation	Period	Extant dating results						
					P	EP	M	N	Me	C	BA
>10200	Forest colonization	Cold dry	Aeolian deposits	P	46	3	2				2
10200–9300	Forest development	Warmer and wetter			1	1					
9300–8300	Forest closure	Warm and wet		EP	4	1	1				
8300–7700	Possible lowland clearance/cultivation	Cycles of warm-dry/cool-wet			1	2			1		
7700–6700	Lowland anthropogenic clearance	of c. 500 year duration,			1	6	1				
6700–6500	Possible montane clearance/grazing	general trend to cool-wet				2					
6500–5500	Agriculture in lowlands (Cerealia)			M/N	1	1	35	3	1	1	
5500–4800					2	8	15	1			
4800–4500	Grazing			N		1	5				
4500–4000	Expansion of small scale deforestation	Drying following weakening	Alluvial accumulations			1	14				
4000–3600	Increased arable yields	of African monsoon				2	12				
3600–3300	Shift from cultivation to grazing.					1	9	1	1		
	Reforestation										
3300–2600	Deforestation, overgrazing	Warm wet	Significant erosion: upland	N/C	3		2	9	10		
2600–2300	Reforestation	(strongly seasonal?)	Some colluviums and	C			2	3	8	2	
2300–1900	Field cultivation		alluviums		1		2	2	3	2	
1900–1500	Progressive deforestation			BA				1	2	14	
1500–100	Contrasting phases: intensive field cultivation/pasture/deforestation/stability/reforestation	Some indications of wetter climate		BA/IA	1			1		1	
100BC–350AD	Reduced grazing and erosional pressure	Less wet		R					1	1	
350–900	Valley deforestation, upland reforestation			Med			3				
900–1050	Large scale deforestation: valleys		Severe valley erosion								
1050–1250	Large scale deforestation: uplands	Warm dry	Severe erosion: upland and valley						1		
1250–1450	Progressive severe soil erosion										
1450–1650	Permanent erosional degradation	Cold wet	Severe upland erosion:	PM							
1650–ca.1800	Forestry plantation	(Little ice age)	alluviums								

used to address questions of provenance, technology, use, and alteration/degradation/weathering (Dias and Prudêncio, 2007). Field- and high resolution- gamma spectrometry (FGS, HRGS) provide daughter radioisotope activities for different sample geometries and are used to evaluate spatial and temporal variability of dose rate (e.g. Trindade et al., 2013).

The Alto Ribatejo is a region of diverse geology, located on the faulting between the Central Iberian Zone (CIZ) and the Ossa Morena Zone (OMZ). River valleys are deeply incised into the Mesozoic Lusitanian Basin and the Lower Tejo Cenozoic Basin (Oliveira et al., 1992), through a partial coverage of Mio-Pliocene fluvial clayey sands (Pais et al., 2012; Ch 5.5). The study region is delimited to the South by the valley of the modern Tejo, and transition to the plains of Alto Alentejo. The present and recent climate is warm-temperate with dry, warm-hot summers, and hence highly seasonal in terms of wetness and moderately seasonal in temperature (codes Csa-Csb according to Köppen-Geiger climate classification, Rubel and Kottek, 2010). Regolith is commonly acidic and highly weathered. Indications from a high altitude lake core ca. 80 km to the North (van der Knaap and van Leeuwen, 1995), are of a fluctuating Holocene climate with phases of landscape activation and stability (Table 1), which was on average rather wetter than present from ca. 9000–3000 BC and slightly wetter than present since ca. 3000 BC. Charred particle analysis has highlighted palaeoclimatic/autogenic changes (Connor et al., 2012), but indicates potential for human impact from ca. 8000 BC. Anthropogenic (local) factors came to dominate climatic (regional) in its pollen assemblages from around the onset of megalithic construction in Iberia at the end of the 5th millennium BC. Substantial landscape clearance is only indicated from the 3rd millennium BC onwards, when the chrono-sequence may

become less precisely relatable to the Alto Ribatejo, but the relationship is renewed with the rapid and regional Roman conquest, indicated by *Castanea Sativa* pollen.

The transition from the Mesolithic to Neolithic and the earliest agriculture near the Iberian Coast has been placed 5600–5400 BC, that for the interior 4900 BC; while the onset of megalithic construction is placed around 4200–4000 BC (Carvalho, 2010; Rowley-Conwy, 2011; Zapata et al., 2004). Archaeologically the Alto Ribatejo region has produced variants on the paradigms of Neolithization. Important among these is a drawing away from focus on coastal spread followed by inland dispersal of people ("cardial model", Zilhão, 1997), towards the possibility of overland spread along river valleys and a balance between the movement of people (replacement) and that of technology/ideas (integration) (Oosterbeek, 2001). The apparently lengthy Mesolithic–Neolithic co-occupation or transition in the coastal regions of Portugal has led to increasing emphasis on Epipalaeolithic communities as the precursors for integrative Neolithization (Carvalho, 2010; Scarre et al., 2003, Table 1), unlike other regions of Atlantic Europe (Scarre, 2007). Radiocarbon and luminescence dates as early as ca. 4000 BC have been reported for megaliths in the Tejo valley and various parts of Portugal (Scarre et al., 2003, Table 2; Scarre and Oosterbeek, 2010; Cruz, 2007, Table 1). How agro-pastoralism in the upper reaches of the Portuguese Tejo valley relates chronologically to evidence from on one hand coastal Portugal, and on the other to central and ultimately eastern Iberia, is important to distinguish between different models (Oosterbeek, 2001). However, there is a preponderance of absolute dating evidence from non-megalithic littoral sites and the nature of the sites and records changes with the landscape: shell middens are absent in-land and early megalithic contexts in this region tend to be aceramic. Despite



adverse conditions at most inland archaeological sites, cases of organic preservation (e.g. Figueiredo, 2007) dominate the current absolute chronological record through  $^{14}\text{C}$  analysis (Table 1). In addition, while megalithic monuments remain an important focus of studies in this region, a range of important site types are recognized and there is a shortage of absolute chronology for archaeological sites related to agro-pastoral activities (Oosterbeek, 2001).

The present study aims to address the lack of absolute chronology for the transition to agricultural societies in the Alto Ribatejo and improve understanding of formation processes in different types of archaeological site in this landscape. Its objectives are firstly to generate new geochronological, geochemical, and mineralogical data for different types of archaeological site related to the transition to agriculture around the Alto Ribatejo, and to use these data to investigate relationships between sample characteristics and their luminescence behaviours. This will be used to establish the suitability of luminescence dating techniques and permit the combination of measured data from heated and unheated artefacts, with field observations and archaeological interpretations, to characterize the types of site encountered in the region and elucidate site formation processes. Based on this analysis, materials and methodologies for future programmes of analysis will be identified.

## 2. Sites and samples

Four different types of feature in the archaeological landscape of the Alto Ribatejo were selected for study (Fig. 1): passage tombs (positive, megalithic; AL, CP), pit fills (negative; QP), a structure represented by a stone scatter layer (SMC), and an *in situ* heated clay structure (FNT). The term regolith is henceforth used generally to indicate material not from heated artefacts.

Anta da Lajinha (AL) and Cabeço dos Pendentes (CP) lie on high ground (ca. 300 m asl.), respectively overlooking tributary valleys of the Ribeira da Isna and Ribeira da Pracana, on Cambrian schists of the Douro-Beiras super group (Oliveira et al., 1992). AL consisted of a small megalithic passage tomb (Fig. 1), encased in a tumulus, ca. 10 m dia., of local highly weathered schist regolith (da Silva, 1939; pH 4.55, C. French, 2006. *pers comm*). A thin organic rich topsoil (Layer A) sealed a clast rich sandy silt (Layer B, upper 25–30 cm), which overlay a reddish brown clay with fewer smaller clasts (<2 cm) and occasional charcoal (Layer C), over bedrock. Six of the eight orthostats and much chamber fill had been excavated/disturbed since the 1930 s (da Silva, 1939). The passage appeared free from recent disturbance but to have been destroyed in antiquity. The remains of another chambered tomb, CP, lie 11.5 km South: its orthostats had been removed, but appeared to have been emplaced on top of a layer of fill (yellowish brown clay, clasts < 2 cm), in a circular hollow cut directly into schist bedrock (Scarre et al., 2011). Undecorated ceramics from various locations at AL indicated prehistoric site usage but were not diagnostic of particular periods. A decorated schist plaque and flint arrowheads from CP indicated site usage in the Chalcolithic. However, the structural forms were suggestive of the Neolithic, as part of the

**Fig. 1.** Site locations and general views of each site, with indications of sampling locations (solid arrows), sampled contexts (dashed arrows), sampling locations in subsequently excavated contexts (point on vertical reference line, AL), and locations of adjunct samples and *in situ* measurements (solid points, QP). AL = Anta da Lajinha, CP = Cabeço dos Pendentes, QP = Quinta do Paço II, SMC = Santa Margarida da Coutada, FNT = Povoado de Fontes. Ridges south of AL and CP are associated with thick quartzite veins in the schists of this area. Incision by the Zêzere and tributaries along faulting in the Porto-Tomar Shear zone is also apparent (and see Murphy and Roberts, 1997, Fig. 2.). Map from LNEG (2013).

earliest stages of megalithic spread across the Tejo. An aim of investigating the sites was to discover whether their construction pre- or post- dated clearance by early farmers, if significant vegetation coverage ever existed in these areas (Scarre et al., 2011). Ten regolith samples were taken from the tumulus, and the passage and chamber fills at AL, and two from the remnants of fills at CP.

Five negative features and an upright menhir were encountered at Quinta do Paço II (QP), Ferreira do Zêzere (Fig. 1), respectively containing and surrounded by series of thin compacted carbonized horizons and hearths, indicating repeated use (Caron et al., 2010). Ceramics from these contexts were indicative of the late Chalcolithic/early Bronze Age, and stone features associated to late Bronze Age/early Iron Age occupation were also recorded in the area. QP lies in the OMZ in an area of upper Proterozoic chloritic and muscovitic schists and amphibolites (Oliveira et al., 1992), with bands of tonalitic gneiss (Chaminé et al., 2003). The regolith consists of dark reddish brown sandy clay and light reddish brown clayey sand respectively. Four ceramic and four sediment samples recovered from the pit fills and substrate (Fig. 1) were analysed, to test whether construction of the pits related to either identified archaeological period or to earlier activity, possibly associated with the menhir, and for inherited/residual luminescence age in the ceramics/fill materials.

Povoado de Santa Margarida da Coutada (SMC) lies at 107 m asl. on gently sloping ground in a presently dry valley above the south bank of the Tejo (Batista, 2004, Fig. 1). Excavation revealed a sub-circular stone scatter (habitation structure; Cruz, 2006), associated with a range of artefact types including apparently *in situ* Chalcolithic ceramics (Fig. 1). The modern topsoil (Layer A) was developed on colluvium (Layer B), which contained the stone scatter/structure (Layer B centre) and was gleyed at its base (Layer C; water table). Apart from the stone scatter layer, the colluvium had a homogeneous aspect with few non-oriented clasts <5 cm: below the stone scatter these included Palaeolithic artefacts. SMC lies on an Upper Miocene argilo-arenitic formation, close to Quaternary Terrace 1 deposits of the Tejo, with Pliocene clayey arenites and conglomerates uphill (Ribeiro et al., 1977). Two ceramic sherds from the structure and two samples from the colluvium bracketing it were analysed, to delimit emplacement of the stones and test the *in situ* nature of the artefact assemblage from them.

Povoado de Fontes (FNT) lies on a gentle slope high on the east bank of the lower Zêzere, 294 m asl. (Fig. 1; Batista, 2004), with localized outcrops of Ordovician schists with quartzite bands, Miocene and Pliocene clayey arenites and conglomerates, and Middle Proterozoic micaschists, gneisses and migmatites (Oliveira et al., 1992; Cruz, 2010). Loose, burnt topsoil (Layer A) covered by quartz pebbles/grit, sealed red-brown colluvial gritty sandy clay (Layer B). Below this, a thin layer of quartz pebbles sealed compact yellow-brown gritty sandy clay with occasional non-oriented stones (3–10 cm) (Layer C), which overlay a very compact grey-brown gritty clay with many large stones (<30 cm) (Layer D). Artefacts encountered in/on Layer A included potsherds indicative of the early- to mid- Neolithic. Layers B and C yielded worked flint, debitage and sherds including coarse corded ware (Neolithic–Chalcolithic transition), and a concentration of quartz pebbles (post hole infill; Cruz, 2010). Founded in the top of Layer D (otherwise sterile) and extending up into Layer C were sub-circular structures of red-brown sandy clay, which appeared heated but otherwise unprocessed. These have been interpreted as ovens or storage silos (Cruz, 2010), or fire places in huts, and may provide direct evidence of early agro-pastoral activities. A regolith sample was taken from Layer C and three blocks were taken from one structure, to date the activity that produced the structure, test whether Layer C was cut by the structure or had accumulated around it, and evaluate how the different ceramic assemblages related to the stratigraphy.

### 3. Methods

Twenty-eight sets of samples for dating (19 regolith and 9 ceramic/heated clay) were taken from 5 archaeological sites (Fig. 1). Samples for ITNLUM 56 to 275 were taken in dry conditions in late summer. Those for ITNLUM 438 to 453 were taken in wet conditions in winter. Regolith samples were taken from previously exposed sections using stainless steel tubes (3.8 cm or 7 cm dia., 15 cm l., ~0.2 or ~1 kg sample). Ceramic sherds (20–40 g, 0.5–1 cm thick, 4–8 cm dia.) and clay-structure samples (90–380 g, 4–8 cm long, ca. 4 cm dia.) had been previously excavated and were received on-site. In all cases a ca. 30 cm length, 8 cm diameter hole was excavated in a location representative of the burial context of the sample (adjunct sample): Field gamma spectrometry (FGS) measurement was conducted *in situ* for 1 h using a 2" × 2" NaI probe with a Target Nanospec or HPI Rainbow MCA, calibrated relative to the Oxford and Gif-sur-Yvette blocks (Richter et al., 2003). For ITNLUM 56 to 275, the integral signal >500 keV was used to obtain the dose rate from gamma radiation. For ITNLUM 438 to 453, regions of interest in each spectrum were used to obtain values for the concentrations of K, Th, and U. Where measurements were made close to the present ground surface when the sample would have been buried deeper in the past (e.g. CP, Fig. 1), the solid angle of terrain detected was estimated and the measured value converted to that for total enclosure.

In the laboratory, water content as a fraction of dry (50 °C) sample mass was measured as received ("field";  $W_f$ ), saturated ( $W_s$ ), and for ITNLUM 438 to 453 following free drainage for 1 h (0 days) to 8 days ( $W_{D0-8}$ ). The time-averaged water content ( $\bar{W}$ ) was constrained based on these values, on the contextual information summarized in Table 1, and on the site descriptions. For all sites except SMC, minimum constraints were assumed to be the average  $W_f$  of the regolith samples taken in summer, and  $W_{D8}$  for ceramics. Maximum assumed constraints were  $W_f$  for samples taken in winter. For ceramics these values were also applied to samples taken in summer,  $W_s/2$  was used for the regolith samples taken in summer. Since SMC was located in a valley bottom close to the water table, the minimum constraint was assumed to be  $W_f$  and the maximum  $W_{D8}$ .

Sample exteriors were removed in subdued light conditions. Part of the "core" of each ceramic was subsampled, dried and milled. The loose sediment adjunct to the dating samples was dried (40 °C) disaggregated, sieved (2 mm), mixed and quartered, then a ca. 50 g subsample was milled. The mineralogy of the milled material was analysed by XRD, using a Philips X'Pert Pro diffractometer, with CuK $\alpha$  radiation, operating at 45 kV and 40 mA. Powder diffractograms were obtained in the 4–60 °2 $\theta$  range, using a 1° divergence slit scanning at 1°/min. Identification of crystalline phases was performed using International Centre for Diffraction Data Powder Diffraction Files (ICDD PDF). Estimation of mineral amounts was obtained by the peak areas of diagnostic reflections of each mineral. Total mineral peak areas of each sample were then converted to 100% in order to obtain rough estimates of mineral percentages and enable comparison between samples.

For INAA, approximately 200 mg of the milled materials was sealed in HDPE phials, which were irradiated in the Portuguese Research Reactor (PRR, IST/CTN), with a thermal neutron flux of  $3.96 \times 10^{12}$  n.cm<sup>-2</sup>.s<sup>-1</sup>,  $\Phi_{epi}/\Phi_{th} = 1.03\%$ ,  $\Phi_{th}/\Phi_{fast} = 29.77$ , in parallel with two standards in identical geometry for each irradiation (GSS1, GSS4, GSS5, GSD9; reference values from Govindaraju, 1994). The samples and standards were analysed using high-resolution gamma spectrometry (HRGS) (Dias and Prudêncio, 2007; Gouveia and Prudêncio, 2000; Prudêncio et al., 2006). The two spectrometers used were a 150 cm<sup>3</sup> HPGe detector (FWHM of 1.9 keV at 1.33 MeV) and a low energy photon detector (LEPD, FWHM of 300 eV

**Table 2**

Calibration doses used in SAR OSL measurement sequences. (R) indicates a repeat point and (IR) indicates a repeat point where the OSL response was measured following infrared exposure to test for the presence of minerals other than quartz (Duller, 2003). OSL was measured at 125 °C for 125 s.

	Reference (ITNLUM_)				
Regenerative dose sequence	273, 274, 275, 438, 439, 440	441, 442, 443, 444, 450, 451, 452, 453	221, 220, 222, 223, 56 <sub>r1</sub> , 57 <sub>r1</sub> , 59 <sub>r1</sub> , 60 <sub>r1</sub>	272	202 <sub>r1</sub> , 203 <sub>r1</sub> , 204 <sub>r1</sub> , 205 <sub>r1</sub> , 206 <sub>r1</sub>
N	–	–	–	–	–
$\beta$	200	160	60	20	59
Z	0	0	0	0	–
$\beta/4$	50	40	15	5	119
$\beta/2$	100	80	30	10	178
2 $\beta$	400	320	120	40	238
4 $\beta$	800	640	240	80	297
Z(R)	0	0	0	0	0
$\beta$ (R)	200	160	60	20	59
$\beta$ (IR)	200	160	60	20	–
$\beta$ test	10	10	10	10	20

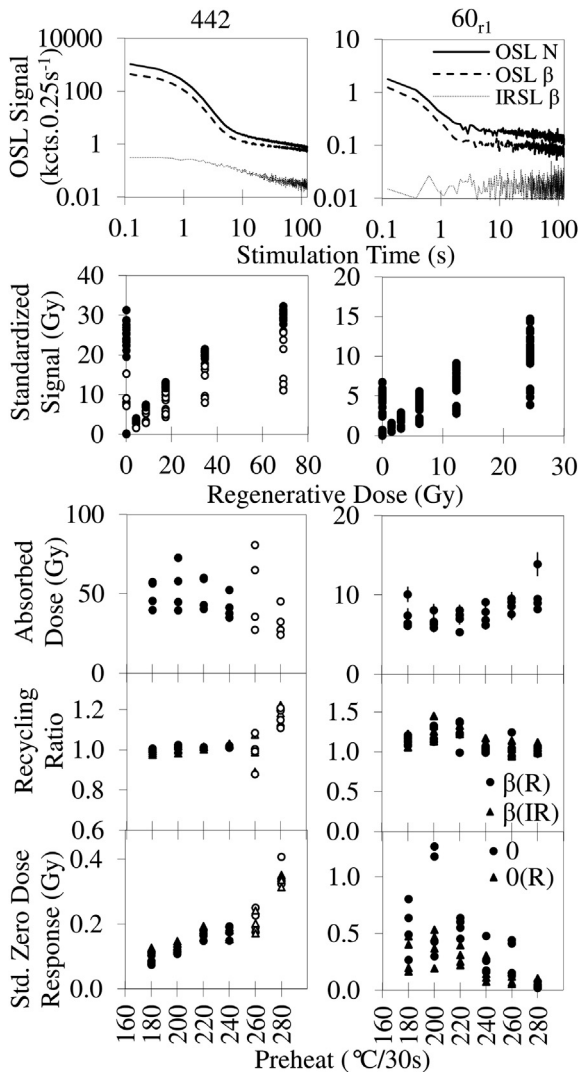


**Fig. 2.** Examples of contrasting OSL behaviour within the SAR protocol (ITNLUM 442, SMC, and ITNLUM 60<sub>r1</sub>, QP). a. N and  $\beta$  OSL, and  $\beta$  IRSL, decay curves for aliquot 11 (preheat 220 °C) from each sample. b. Standardized dose responses (Roberts and Duller, 2004) of all aliquots. c. D vs. preheat. d. Recycling ratio ( $I_{\beta(R)}/I_{\beta}$ ) and IR recycling ratio ( $I_{\beta(IR)}/I_{\beta}$ ) vs. preheat. e. Zero-dose responses,  $D_{\beta}(I_{\beta}/I_{\beta})$  and  $D_{\beta}(I_{\beta(R)}/I_{\beta})$  vs. preheat.

at 5.9 keV, 550 eV at 122 keV), both with Canberra 2020 amplifiers and Accuspec B MCAs. Absolute and chondrite normalized (Anders and Grevesse, 1989) concentrations of 27 elements were compared with upper continental crust (UCC) and post-Archaean Australian Shale (PAAS) averages (Rudnick and Gao, 2003; Taylor and McLennan, 1985) to identify enrichment/depletion. Comparison of incompatible/compatible element ratios using relatively insoluble and hence chemically immobile elements, sensitive to source composition, was then conducted to indicate distinctions between felsic and mafic source materials (Taylor and McLennan, 1985).

Infinite matrix dose rates ( $\dot{D}$ ) from alpha, beta and gamma radiation were calculated from elemental concentrations of K, Rb, Th and U measured by FGS and INAA, using conversion factors from Adamiec and Aitken (1998) and following correction for  $W_f$  in the case of FGS. These values were corrected for  $\bar{W}$  based on Zimmerman (1971). The self-dose of the quartz grains was assumed negligible (Burbidge et al., 2009). The time averaged cosmic dose rate was calculated from Prescott and Stephan (1982) and Prescott and Hutton (1988), taking into account the contribution from the soft component and the expected history of accumulation and erosion at each site and assuming bulk density of 1.6 g.cm<sup>-3</sup>. These values were combined using approximations of the geometry represented by each measurement or sample, to estimate the dose rate to the HF etched cores of the quartz grains measured using OSL:  $\dot{D}$ . FGS results were assumed to represent an infinite matrix around the sample. INAA values for material from the cylindrical holes excavated for FGS and from regolith samples taken in tubes, were assumed to represent spheres of diameter =  $2/(1/\text{sample length} + 1/\text{sample diameter})$ . Blocks of heated clay were approximated in the same way, assuming a cylinder 30 cm long and 8 cm in diameter to represent the portion of the structure (rather than the sampled fragment) that would have contributed the majority of self-gamma dose while buried. Wide, flat ceramic sherds were approximated as infinite layers of their measured thickness. The quartz grains were assumed to be spheres of  $(90 + 160)/2 = 125 \mu\text{m}$  diameter, HF attack was assumed to have removed  $6(\pm 3) \mu\text{m}$  from their exteriors. Bulk density was calculated where possible, but otherwise assumed to be 1.6 g.cm<sup>-3</sup> for samples and 2.65 g.cm<sup>-3</sup> for grains. Attenuation factors, proportions of self-dose, and ranges, were from Adamiec and Aitken (1998), Aitken (1985), Bell (1979), Bell and Zimmerman (1978), Fleming (1970), Krane (1988), Mejdahl (1979, 1983), Stabin and da Luz (2002) and NIST ESTAR (2009). These were applied on a radioelement- and radiation type- specific basis where element concentrations were available, or as radioelement averaged but radiation type specific factors.

For luminescence measurements, the central, light protected part of each sample was disaggregated then wet sieved (90–160  $\mu\text{m}$ ). To obtain quartz, the sieved fraction was treated with H<sub>2</sub>O<sub>2</sub> and HCl (both 10%, 10 min), centrifuged in sodium heteropolytungstate solution, the 2.62–2.74 g.cm<sup>-3</sup> fraction was attacked with HF (40%, 40 min) then washed in HCl (10% 10 min), then re-sieved wet at 90  $\mu\text{m}$ . The resultant material was checked under a binocular microscope, to verify the type and form of mineral grains obtained, including the efficiency of the separation procedure in isolating quartz of the desired grain-size. It was then tested using a measurement sequence including optical stimulation at 830 or 880 nm (“IRSL”) and 470 nm (“OSL”) and TSL (rt – 500 °C), adapted from Burbidge et al. (2007). This was designed to check natural signal levels, sensitivity to dose, predose sensitization, approximate absorbed dose levels and evidence for heating, in quartz and any non-quartz minerals present, and so to indicate requirements for any further preparatory treatment and to help select and design an appropriate measurement protocol. Density separation and HF attack was repeated for ITNLUM 443, 444, 451, 452, and 453.

For evaluation of  $D$  using OSL (470 nm), monolayers of grains *ca.* 5 mm diameter were fixed on 12–24 stainless steel cups per sample using silicone oil (*ca.* 500–2000 grains per cup, depending on quantity of quartz recovered). OSL measurements were made using a SAR protocol (Murray and Wintle, 2000), with Hoya U-340 (50%  $T_{\max}$  280–370 nm) detection filters in Risø DA-15 and -20 TL-OSL readers, with  $^{90}\text{Sr}/^{90}\text{Y}$   $\beta$  irradiators giving 0.084 and 0.109 ( $\pm 2\%$ )  $\text{Gy}\cdot\text{s}^{-1}$  to these samples. Each cup was measured using the sequence of regenerative calibration doses indicated in Table 2.  $\beta$  was selected for each site based on initial tests, and a  $\log_2$  dose scale used, except for reanalysed results from samples ITNLUM 202 to 206. Signals were obtained by subtracting the average count rate in the last 25 s of measurement from that in the first 5 s, which included the majority of the rapidly decaying OSL (Fig. 2). Signals normalized to subsequent test dose (Table 2) responses were fitted with single saturating exponential curves, and the absorbed dose represented by each signal  $N$  was interpolated. Results were rejected where systematic effects on absorbed dose as a function of preheat temperature and/or the reproducibility of the repeat point and zero-dose responses were considered significant relative to statistical uncertainties. The remaining results were analysed statistically in normal space using a weighted maximum likelihood estimate for a single population to estimate the absorbed dose for the sample as a whole,  $D$ . In less scattered cases, the analysis assumed the observed distribution to represent the sum of measured statistical uncertainties and underlying scatter, with the aim of describing the “true” form of the data (e.g. the CAM of Galbraith et al., 1999). This did not work well for very scattered results, but the weighted mean, weighted to the inverse variance on each measurement, provided a reasonable descriptor of the location of the main grouping in these datasets.

#### 4. Results

Luminescence date estimates were produced for 28 samples (19 regolith and 9 ceramic/heated clay samples) from 5 archaeological sites (Table 3; Table 4; Fig. 1), from 62 sets of geochemical/

mineralogical/dosimetric measurements (19 FGS, Table 3; 14 XRD, Table 5; 29 INAA, Table 6), 29 sets of water content measurements (Table 3; Fig. 4) and 28 sets of OSL analyses (Table 4; Fig. 3; Fig. 2).

The cups of quartz grains measured by OSL exhibited strong differences in their sensitivity to radiation, both within and between samples. Lowest values were obtained for the regolith from QP; highest for the regolith from SMC ( $\bar{T}_N = 0.3\text{--}2$  and 16 kcts per Gy; Fig. 3; Fig. 2). Ceramic samples were smaller but yielded moderate to high signals ( $\bar{T}_N = 1\text{--}14$  kcts per Gy), and exhibited little scatter in absorbed dose estimates, where systematic variations with measurement conditions were not evident (std. dev. accepted = 4–6%; 13% for ITNLUM 223). Systematic effects on absorbed dose at high preheats were observed in some groups of samples: increased scatter at FNT, high estimates at AL, and low estimates for the regolith from SMC (Fig. 2). Accepted results for some regolith samples and those from the clay structure also exhibited little scatter (2–7%, Fig. 3, ITNLUM 59<sub>r1</sub>, 202-6<sub>r1</sub>, 273, 275, 438-9, 450-3). Archaeological heating of the clay structure at FNT was verified by the ratio of absorbed dose estimates from OSL and TSL in the initial tests: 15:20 Gy, vs. 10:40 Gy for the unheated sediment, but their radiation sensitivities were similar (Fig. 3). By contrast the regolith samples ITNLUM 56<sub>r1</sub>, 60<sub>r1</sub>, 272, 441 and 442 exhibited significant scatter in absorbed dose (std. dev. accepted = 18–32%), and the estimates of  $D$  for these samples are considered less reliable than the other results (“?” in Table 4). The luminescence signals of these samples’ constituent sand grains may not have been reset at the same time; though at QP it could be a consequence of low signal levels.

The field water contents of the regolith ( $W_f$ , Table 3) ranged from 0.002 to 0.33 g/g, high values related to sampling in winter and *vice versa*. Differences in saturation level and initial drainage rate related principally to stoniness, but drainage was then slow in all regolith samples, reflecting the presence of fine material. Free-drainage ( $W_{D0-8}$ ) measurements indicated that the regolith could retain water contents between *ca.* 0.18 to 0.35 for significant periods (Fig. 4), but the summer  $W_f$  values were consistently less than 0.02 (Table 3). This is less than air-dry values for silts and clays (Rowell, 1994; Section 5.1), reflecting low humidity and strong

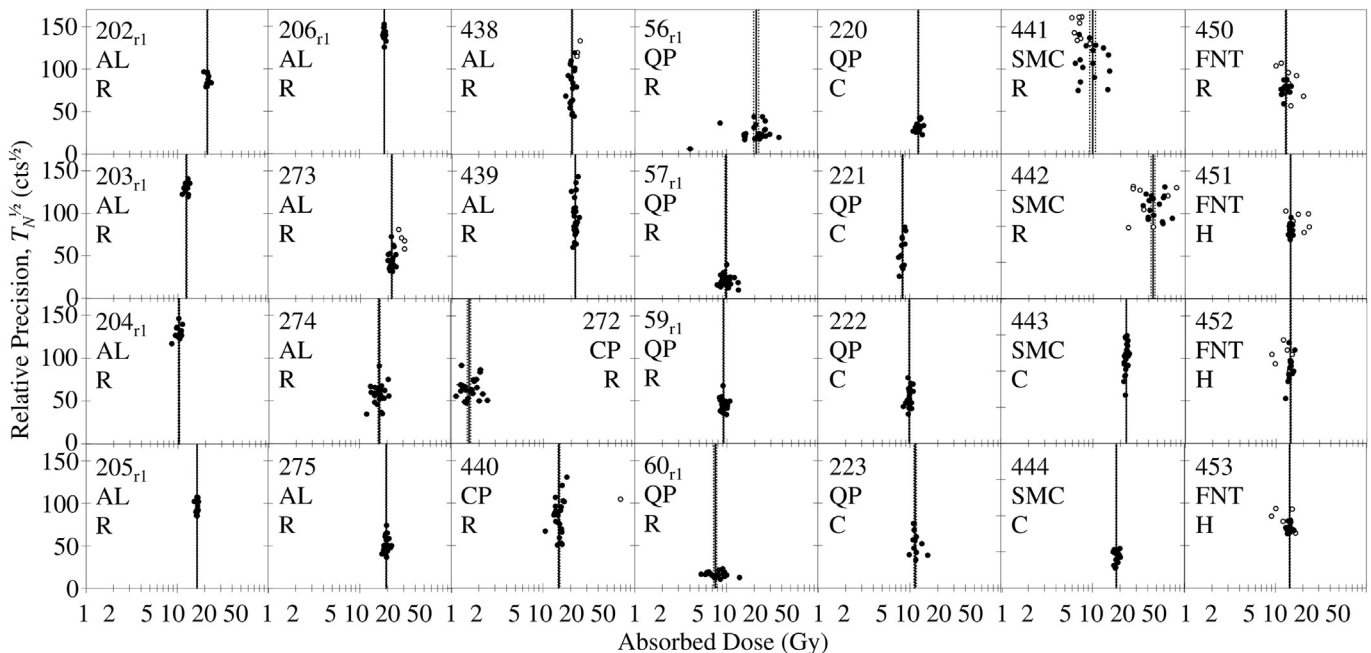


Fig. 3. Absorbed doses,  $D$ , for each aliquot of each sample, vs. the square root of the first test dose response “ $T_N$ ”.  $T_N^{1/2}$  is a proxy for precision based on counting statistics that is largely independent of  $D$  (Burbidge, 2003). R = regolith, C = ceramic, H = heated clay.

**Table 3**  
Results of water content, radiometric, and geochemical analyses used in dose rate calculation.

Reference (ITNLUM) <sup>a</sup>	FGS, <i>In Situ</i> <sup>b</sup>				INAA sediment/soil					INAA ceramic/heated clay							
	$\gamma \pm \sigma_\gamma$ (mGy a <sup>-1</sup> )			Solid angle	$W_f$	Ref.	K	Rb	Th	U	$\bar{W}$	Ref.	K	Rb	Th	U	$\bar{W}$
	K (%) <sup>c</sup>	Th (ppm) <sup>c</sup>	U (ppm) <sup>c</sup>														
<b>Anta da Lajinha (AL)</b>																	
204 <sub>r1</sub>	0.7	±	0.1	4	0.01	A6/602	1.9	112	11	2.7	0.07	–	–	–	–	–	–
203 <sub>r1</sub>	0.8	±	0.1	4	0.01	A6/601	1.9	116	11	2.8	0.07	–	–	–	–	–	–
274	1.0	±	0.1	4	0.02	A7/294	2.2	125	11	2.7	0.08	–	–	–	–	–	–
205 <sub>r1</sub>	0.8	±	0.1	4	0.01	A6/603	2.0	121	11	2.8	0.07	–	–	–	–	–	–
206 <sub>r1</sub>	0.8	±	0.1	4	0.01	A6/604	2.1	96	9	2.6	0.08	–	–	–	–	–	–
438	1.7	8.2	2.3	4	0.17	A9/190	2.4	130	11	2.7	0.10	–	–	–	–	–	–
275	1.0	±	0.1	3.9	0.02	A7/295	2.0	120	11	2.7	0.07	–	–	–	–	–	–
202 <sub>r1</sub>	0.8	±	0.1	4	0.01	A6/600	2.3	134	12	3.0	0.07	–	–	–	–	–	–
273	1.0	±	0.1	4	0.02	A7/293	2.3	129	12	2.9	0.07	–	–	–	–	–	–
439	1.7	8.2	2.2	4	0.17	A9/191	2.0	118	11	2.5	0.09	–	–	–	–	–	–
<b>Cabeço dos Pendentes (CP)</b>																	
272	0.6	±	0.1	3	0.02	A7/292	1.6	94	9	2.5	0.08	–	–	–	–	–	–
440	1.5	6.5	2.2	3	0.33	A9/192	2.3	124	10	2.8	0.17	–	–	–	–	–	–
<b>Quinta do Paço II (QP)</b>																	
221	0.7	±	0.1	4	0.002	A6/069&72	1.7	110	11	2.2	0.07	A6/734	3.3	133	11	2.8	0.06
60 <sub>r1</sub>	0.7	±	0.1	4	0.002	A6/072	1.6	99	13	2.2	0.07	–	–	–	–	–	–
223	0.7	±	0.1	4	0.002	A6/071	1.7	123	11	1.9	0.07	A6/736	3.2	109	20	5.6	0.06
222	0.7	±	0.1	4	0.002	A6/070	1.9	107	9	2.2	0.07	A6/735	2.7	152	10	3.0	0.06
57 <sub>r1</sub>	0.7	±	0.1	4	0.002	A6/069	1.8	121	10	2.2	0.07	–	–	–	–	–	–
59 <sub>r1</sub>	0.7	±	0.1	4	0.002	A6/071	1.7	123	11	1.9	0.07	–	–	–	–	–	–
220	0.5	±	0.0	3	0.002	A6/067&68	1.9	115	10	3.5	0.07	A6/733	2.8	122	13	3.3	0.06
56 <sub>r1</sub>	0.5	±	0.0	3	0.002	A6/068	1.7	109	10	3.3	0.07	–	–	–	–	–	–
<b>Santa Margarida da Coutada (SMC)</b>																	
441	1.6	11	2.7	3.85	0.12	A9/193	2.1	113	15	2.9	0.14	–	–	–	–	–	–
444	1.7	11	2.5	3.8	0.15	A9/196	2.2	114	16	2.9	0.12	A9/196	2.3	131	11	3.4	0.07
443	1.7	11	2.5	3.8	0.15	A9/195	2.2	114	16	2.9	0.12	A9/195	2.4	95	31	3.0	0.06
442	1.8	10	2.2	3.75	0.17	A9/194	2.3	115	17	3.0	0.11	–	–	–	–	–	–
<b>Povoado de Fontes (FNT)</b>																	
450	0.4	4.7	1.3	3.9	0.21	A9/202	0.6	43	8	2.1	0.11	–	–	–	–	–	–
452	0.4	4.7	1.3	3.9	0.21	A9/202	0.6	43	8	2.1	0.11	A9/203	0.2	27	11	1.7	0.05
451	0.4	4.7	1.3	3.9	0.21	A9/202	0.6	43	8	2.1	0.11	A9/204	0.2	23	10	1.7	0.05
453	0.4	4.7	1.3	3.9	0.21	A9/202	0.6	43	8	2.1	0.11	A9/205	0.3	27	7	1.4	0.05

<sup>a</sup> ITNLUM<sub>r1</sub> are revised estimates of previously issued results.

<sup>b</sup>  $\gamma \pm \sigma_\gamma$  using the threshold method; K, Th, U using the windows method; both sets as measured, i.e. not corrected for geometry or *in situ* water content.

<sup>c</sup> Average uncertainties for K = 8% and 4%, Rb = - and 6%, Th = 13% and 4%, U = 14% and 12%; for FGS and INAA respectively.

<sup>d</sup> Water content as a fraction of dry sediment mass  $W_f$  = measured field water content,  $\bar{W}$  = estimated time averaged water content. Average uncertainty estimated for  $\bar{W}$  was 0.06.

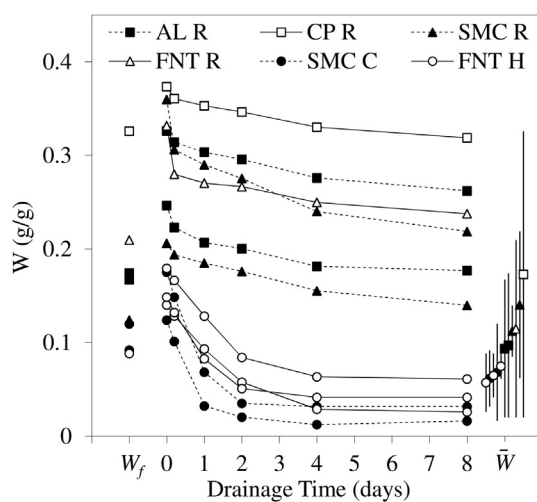


**Fig. 4.** Field water content ( $W_f$ ), saturated overnight and subsequent free-drainage characteristics, and estimates of the time-averaged water content ( $\bar{W}$ ), as a fraction of dry sample mass, for selected samples of regolith (R), ceramic (C) and heated clay (H).

evapotranspiration. Ceramics and heated clay exhibited lower saturation ( $W_s$ ) and drained more rapidly. For the hilltop/slope sites the average of summer and drained values were considered to slightly overestimate the present annual average, and so to be appropriate to account for long term variations (Table 1). For a valley site (SMC) the average of winter and drained water contents were used. Estimates of  $\bar{W}$  were on average 0.09 g/g for the regolith and 0.07 g/g for ceramics and heated clays (Table 3). Uncertainties on  $\bar{W}$  were as high as 0.15 g/g for the most water retentive regolith samples. In the present samples a change of 0.01 g/g in  $\bar{W}$  caused differences in age of on average 1.03( $\pm 0.01$ )% (c.f. Aitken, 1985).

Estimated mineral abundances in selected samples from the different sites are listed in Table 5. The materials studied consist mainly of quartz, alkali feldspars (K-feldspar and Na-rich plagioclase) and mica, which is more abundant in samples from QP. The regolith from QP also contained abundant kaolinite and traces of hematite and anatase. Traces of hematite were observed in samples from SMC and FNT. Chlorite (clinoclone type) occurs in all samples analysed from AL and CP and in one sample from FNT. The samples from SMC have the highest proportion of alkali feldspars and samples from FNT are the richest in quartz.

The majority of element concentrations, as determined by INAA, in the studied materials are between 0.5 and 2 times UCC (Table 6).

**Table 4**  
Samples, contexts, luminescence measurements, dosimetric calculations, and calendar dates.

Reference (ITNLUM <sub>r1</sub> ) <sup>a</sup>	Type <sup>b</sup>	Context (#)	Depth <sup>c</sup> (cm)	Dose rate			OSL, quartz		Absorbed dose			Calendar date		
				$\dot{D}$ (mGy a <sup>-1</sup> )	$\sigma_D$	(= </>/?) <sup>d</sup>	Accepted/ measured	Statistical analysis <sup>e</sup>	$D$ (Gy)	$\sigma_D^f$	(= </>/?) <sup>d</sup>	Date	$\sigma_{date}$	BC/AD
<b>Anta da Lajinha (AL)</b>														
204 <sub>r1</sub>	R	Tumulus (18)	20	3.05	0.13	=	15/15	CAM	10.2	0.2	<	1350	170	BC
203 <sub>r1</sub>	R	Tumulus (37)	40	3.12	0.13	=	12/12	CAM	12.3	0.2	=	2000	200	BC
274	R	Tumulus (40)	40	3.35	0.14	=	24/24	CAM	16.4	0.4	=	2900	300	BC
205 <sub>r1</sub>	R	Passage (40)	20	3.18	0.14	=	15/15	CAM	16.5	0.1	=	3200	300	BC
206 <sub>r1</sub>	R	Chamber (40)	30	3.19	0.14	=	15/15	CAM	18.6	0.1	=	3800	300	BC
438	R	Tumulus base (68)	70	3.57	0.16	=	20/24	CAM	20.7	0.3	=	3800	300	BC
275	R	Chamber floor (90)	90	3.22	0.14	=	24/24	CAM	19.3	0.2	=	4000	300	BC
202 <sub>r1</sub>	R	Tumulus base (43)	70	3.44	0.15	=	12/12	CAM	21.2	0.2	=	4200	300	BC
273	R	Passage (30)	60	3.49	0.14	=	20/24	CAM	21.9	0.3	=	4300	300	BC
439	R	Passage fill (100)	100	3.21	0.14	=	24/24	CAM	22.1	0.2	=	4900	300	BC
<b>Cabeço dos Pendentes (CP)</b>														
272	R	Chamber periphery (25)	10	2.83	0.11	=	24/24	WM	1.6	0.1	?	1460	30	AD
440	R	Chamber fill (4)	25	3.50	0.23	?	23/24	CAM	14.9	0.3	=	2300	300	BC
<b>Quinta do Paço II (QP)</b>														
221	C	Pit Fill (6)	80	3.58	0.14	=	12/12	CAM	8.4	0.1	=	330	110	BC
60 <sub>r1</sub>	R	Pit Bank (by 6)	60	2.77	0.13	=	24/24	CAM	7.5	0.3	?	700	200	BC
223	C	Pit Fill (17)	90	4.11	0.19	=	12/12	WM	11.4	0.3	=	750	160	BC
222	C	Pit Fill (3c)	90	3.26	0.14	=	24/24	CAM	9.8	0.1	=	1010	140	BC
57 <sub>r1</sub>	R	Pit Fill (6)	90	2.87	0.13	=	24/24	CAM	9.7	0.2	=	1400	200	BC
59 <sub>r1</sub>	R	Pit Fill (17)	100	2.72	0.12	=	24/24	CAM	9.2	0.1	=	1400	200	BC
220	C	Pit Fill (1)	40	3.27	0.13	=	24/24	CAM	12.5	0.2	=	1820	180	BC
56 <sub>r1</sub>	R	Substrate (by 1)	40	2.90	0.14	=	24/24	CAM	21.1	1.3	?	5300	600	BC
<b>Santa Margarida da Coutada (SMC)</b>														
441	R	Colluvium (Bu)	26	3.52	0.16	=	16/24	WM	9.9	0.7	?	800	200	BC
444	C	Stone Scatter (Bc)	38	3.59	0.15	=	24/24	CAM	18.2	0.2	=	3100	200	BC
443	C		38	4.02	0.17	?	24/24	CAM	23.0	0.2	=	3700	300	BC
442	R	Colluvium (Bl)	55	3.88	0.15	=	16/24	WM	45	2	?	9500	800	BC
<b>Povoado de Fontes (FNT)</b>														
450	R	Colluvium/Soil (C)	25	1.67	0.09	=	16/24	CAM	12.9	0.2	=	5700	500	BC
452	H		25	1.44	0.08	=	16/24	CAM	14.4	0.2	=	8000	600	BC
451	H	Clay Structure (25)	25	1.43	0.09	=	16/24	CAM	14.6	0.1	=	8100	600	BC
453	H		25	1.35	0.07	=	16/24	CAM	14.3	0.2	=	8600	600	BC

<sup>a</sup> ITNLUM<sub>r1</sub> are revised estimates of previously issued results.

<sup>b</sup> R = Regolith, C = Ceramic, H = Heated Clay.

<sup>c</sup> Below (inferred) pre-excavation ground level.

<sup>d</sup> Summary assessments of dosimetry and luminescence results. = |</>/? : thought to equal/overestimate/underestimate the most representative value, within quoted uncertainties. ? : potentially outwith uncertainties.

<sup>e</sup> WM = Weighted Mean ( $1/s^2$ ); CAM = "Central Age Model" (Galbraith et al., 1999).

<sup>f</sup> Statistical uncertainty of quoted value, from data dispersion; source calibration uncertainty was incorporated for age calculation.

The main exceptions are low levels of Na (0.015–0.45 × UCC: 0.04–2.45 ppm) and enrichment in Br (2–17 × UCC: 0.9–28 ppm). Patterns of chondrite normalized rare earth element (REE) in the samples are similar to UCC and PAAS: they are all light REE enriched with a negative Eu anomaly. Total REE concentrations in UCC and PAAS are 130 and 160 ppm respectively but vary from 54 to 260 ppm in the studied samples: highest values from the ceramic sherds, similar moderate values for regolith from AL, CP, QP and SMC, and low values from FNT (Table 6). Both the regolith and structure at FNT exhibited low levels of most elements except Br and As. The regolith from AL exhibited high concentrations of the semi-metals As and Sb. Relatively high levels of Sb were also found at CP. The regolith from SMC exhibited relatively low levels of transition metals (Fe, Sc, Co and Zn), As, Ga and Br. The ceramic sherds from SMC and QP exhibited elevated levels of light rare earth elements, Th, Zr and Ga, and higher levels of Na than the other studied samples. Both regolith and ceramics from QP were enriched in Cs. The regolith from this site displayed the lowest enrichment in Br observed at any of the sites. Some samples from SMC, and FNT exhibit La/Sc and Th/Sc ratios much greater than UCC, indicating a felsic source (granites).

K, Th and U concentrations in the samples (Table 3) were on average 1.5%, 9.0 ppm and 2.2 ppm for *in situ* FGS measurements,

and 1.9%, 12 ppm and 2.7 ppm for INAA. Regolith and ceramics/heated clay yielded similar averages but the latter exhibited greater variability. Measured concentrations from FGS are lower than those for INAA largely as a function of *in situ* water ( $W_p$ ) and measurement geometry (Solid Angle, Table 3), which were included in the calculation of  $\dot{D}$ . Cosmic dose rate estimates ranged from 0.19 to 0.28 mGy.a<sup>-1</sup>. Following correction for  $\bar{W}$ ,  $\dot{D}$  averaged 3.3(±0.4) mGy.a<sup>-1</sup> at AL, CP, QP and SMC, and 1.5(±0.1) mGy.a<sup>-1</sup> at FNT, with contributions of Alpha, Beta, Gamma and Cosmic radiation of 2(±1)%, 58(±7)%, 32(±4)%, and 8(±4)%.  $D$  ranged from 10 to 22 Gy at AL, 1.6–15 Gy at CP, 8–21 Gy at QP, 10–45 Gy at SMC, and 13–15 Gy at FNT (Table 4). These produced calendar date estimates from 1350 to 4900 BC at AL, 1460 AD and 2200 BC at CP, 330 to 5300 BC at QP, 800 to 9500 BC at SMC, and 5700 to 8600 BC at FNT, with uncertainties from 4 to 9% at 1 $\sigma$ .

## 5. Discussion

High OSL radiation sensitivity was observed in the quartz from SMC and FNT (heated and unheated), signals from AL and CP were also moderate to high, whereas the sensitivity of samples from QP was lower (Fig. 3). The higher sensitivity samples also tended to exhibit greater effects of high preheats on  $D$  evaluation (280 °C;

Fig. 2). Removal of compensating alkali ions from Al centres in quartz can increase its radiation sensitivity (Martini et al., 1987). This can be achieved through heating, or leaching during weathering and transport either recently or in the geological past: low Na relative to UCC, but similar K, in the regolith at all sites suggests partitioning during weathering of felsic/coarse material (White, 2008).

Most geochemical differences between sites and samples appear related to mineralogical composition (Table 5). Higher levels of Cs were observed in mica-rich samples from QP. Higher levels of Na were observed in ceramic sherds richer in alkali feldspars. Both regolith and structure at FNT exhibit the lowest average elemental concentrations in the present study: this is considered to reflect dilution by quartz and appears strongest in the structure. The local geology of FNT and SMC contains Miocene and Pliocene clayey arenite units derived largely from the CIZ by the palaeoTejo (Pais et al., 2012; Ch 5.5). The felsic signature of samples from these sites (Table 6) may relate to their original source material including granites of the CIZ (e.g. Villaseca et al., 2009). Weak Br enrichment in the regolith at SMC and particularly QP indicates relatively low anthropogenic influence on their composition (Prudêncio et al., 2006; Trindade et al., 2011). Enrichments in Sb at AL and CP, and As at AL and FNT, may relate to mineralization associated with hydrothermal activity in the shear zone on which the study area is located (Ortega et al., 1996).

### 5.1. Radionuclide mobility

INAA measures the concentration of the parent radionuclide while FGS measures emissions from the post-<sup>222</sup>Rn part of the U decay chain, from a large volume, so concordant results can indicate both that the INAA samples are geostatistically representative and that Rn escape *in situ* was not significant. This appears to be the case for the regolith where elemental concentrations were estimated from the FGS data (Table 3). Since the FGS crosscheck does not apply to the ceramic/heated clay samples, sample ITNLUM 451 was tested for maximum potential radon loss. 100 g of dried disaggregated material was measured by HRGS (without neutron activation) shortly after sealing its container, so post-Rn isotopes did not have time to equilibrate. The results were calibrated relative to sealed equilibrated samples of the standards used for INAA

(Section 3). Apparent U concentration was  $1.72(\pm 0.04)$  ppm for pre-<sup>222</sup>Rn emissions from <sup>234</sup>Th and <sup>226</sup>Ra(+<sup>235</sup>U),  $1.30(\pm 0.07)$  ppm from <sup>214</sup>Pb and <sup>214</sup>Bi, and  $1.3(\pm 0.3)$  ppm from <sup>210</sup>Pb. These indicate 24% radon loss and the similar value for <sup>210</sup>Pb ( $t_{1/2} = 22$  a) indicates that this may be relevant to the *in situ* sample condition in recent decades. K and Th were  $0.24(\pm 0.02)$  ppm and  $7.2(\pm 0.2)$  ppm.

The relative concentrations of period 4 transition metals in regolith and structure are variable (Table 6). However, when Sc normalized data (Dias and Prudêncio, 2008) from the structure are compared with the regolith of FNT and with the other sites, K and Zn appear consistently depleted (1.6–2 times). The land surface in which the structure was formed may already have been depleted in K, but if leaching of 50% occurred since the heating event being dated it would imply that the original dose rate ( $\dot{D}_1$ ) for ITNLUM 451 was 10% higher than from measured INAA analyses ( $\dot{D}_2$ ). Since the structure was covered by sediment of higher K content from ca. 5700 BC, it is assumed that any leaching was then inhibited and that the measured K concentrations are applicable during this period ( $P_2$ ). The maximum effect of K loss is then obtained if it occurred at the end of the preceding period ( $P_1$ ), so that  $P_1 = (D - P_2\dot{D}_2)/\dot{D}_1$  (c.f., Zacharias et al., 2007; where the age was known *a priori*).

Estimates of both  $\dot{D}$  (from INAA) and  $D$ , for the different samples from the clay structure are within  $1\sigma$  of each other (Table 4). Calculation of a single result using averaged measurements of K, Th and pre-Rn U gives a date estimate of  $8300(\pm 600)$ BC. Based on the INAA data, modelled K loss gives an average across the samples of 8000 BC, whereas weighted pre- and post-Rn U contributions from the HRGS result gives 8900 BC. Comparison of radiometric, geochemical, mineralogical and chrono-stratigraphic data for this sample and context indicates that effects of methodological differences and radionuclide mobility lie within estimated overall uncertainties. However, in other soils and clays from north-central Portugal, continual weathering and local contrasts in radionuclide concentration have been found to produce differences in dose rate of 30% and 300%, due to K leaching and Ra uptake or Rn loss, respectively (Trindade et al., 2013).

Evaluation of such effects in ceramic sherds may require intensive comparative elemental analyses, ideally including examples of unaltered material (Zacharias et al., 2007). The sherds analysed in the present study were of plain coarse-ware. Those from QP included broader thinner pieces apparently encountered *in situ*. The assemblage at SMC was considered *in situ* but the dated sherds were narrower and thicker and may have been sufficiently robust to have been transported and redeposited. However, K and U concentrations in the sherds from both QP and SMC were on average 1.5 times those of their burial contexts, *i.e.* chemical gradients were generally small. Th/U ratios are within 0.8–1.5 times UCC, with the exception of a high Th content sherd from SMC (A9/195; ITNLUM 443). This yielded the older date estimate from SMC: the difference from the other sherd in both age and Th/U would be consistent with an underestimate of ca. 4.5 ppm U (*i.e.* 3/5), though spatial variations in Th content could also cause the dose rate difference and may be more probable given the observed elevated concentration.

### 5.2. Summary of dating analyses

Interpretations of the luminescence dating results listed in Table 4 illustrate that their chronological meaning, and meaningfulness, differs strongly between samples and contexts (Table 7). For regolith samples, interpretations differ principally according to the event that is considered to be being dated. Dating results *per se* from the heated artefacts carry the broad implication of human presence in an area at a particular time, regardless of context.

**Table 5**  
Mineralogical results obtained by XRD for selected samples in Table 3. Q = Quartz, K = Kaolinite, M = Mica, C = Chlorite, KF = K-feldspar, P = Plagioclase, A = Anatase, H = Hematite. Sample type: R = regolith, C = ceramic, H = heated clay.

Sample	Type	Q	K	M	C	KF	P	A	H
Anta da Lajinha (AL)									
A7/295	R	+++	–	(+)	(+)	(+)	+	–	–
A9/190	R	+++	–	(+)	(+)	(+)	(+)	–	–
A9/191	R	+++	–	(+)	+	(+)	(+)	–	–
Cabeço dos Pendentes (CP)									
A9/192	R	+++	–	(+)	(+)	(+)	(+)	–	–
Quinta do Paço II (QP)									
A6/068	R	+++	++	+	–	(+)	–	+	(+)
A6/070	R	+++	++	++	–	(+)	–	–	–
A6/072	R	+++	++	+	–	(+)	–	–	–
A6/733	C	+++	–	(+)	–	+	(+)	(+)	–
A6/735	C	+++	–	+++	–	–	++	–	–
Santa Margarida da Coutada (SMC)									
A9/193	R	+++	–	(+)	–	+	(+)	–	(+)
A9/195	C	+++	–	(+)	–	+++	(+)	–	(+)
A9/196	C	+++	–	++	–	–	++	–	–
Povoado de Fontes (FNT)									
A9/202	R	+++	–	(+)	(+)	(+)	(+)	–	–
A9/203	H	+++	–	–	–	–	(+)	–	(+)

**Table 6**  
Element concentrations and oxide % of major elements in samples of regolith (R), ceramic (C), and heated clay (H) from each site determined by INAA, with upper continental crust (UCC) and post-Archaean Australian Shale (PAAS) averages from Rudnick and Gao (2003) and Taylor and McLennan (1985). INAA samples are related to luminescence results (ITNLUM) in Tables 3 and 5.

Sample	Type	Concentration (ppm)																										
		Oxide (%)					Element (%)																					
		Na <sub>2</sub> O	K <sub>2</sub> O	Fe <sub>2</sub> O <sub>3</sub> T	Sc	Cr	Co	Zn	Ga	As	Br	Rb	Zr	Sb	Cs	Ba	La	Ce	Nd	Sm	Eu	Tb	Yb	Lu	Hf	Ta	Th	U
Anta da Lajinha (AL)																												
A6/600	R	0.3	2.8	7.0	17	89	22	97	20	26	15	134	199	3.0	5.6	428	41	83	40	7.3	1.5	1.0	3.4	0.5	6.5	1.2	12	3.0
A6/601	R	0.3	2.3	6.3	16	95	12	85	20	18	13	116	205	3.6	4.7	365	38	76	32	6.6	1.4	0.9	3.4	0.5	7.1	1.1	11	2.8
A6/602	R	0.3	2.3	6.5	16	95	12	87	20	19	24	112	181	3.7	4.7	361	37	74	31	6.6	1.4	1.0	3.4	0.5	6.8	1.1	11	2.7
A6/603	R	0.4	2.4	6.6	16	94	16	90	22	22	10	121	223	3.4	5.0	364	43	82	39	7.0	1.4	1.0	3.4	0.5	6.9	1.2	11	2.8
A6/604	R	0.7	2.6	5.8	16	93	10	89	21	13	5	96	200	3.3	3.7	377	35	68	35	6.2	1.3	0.8	3.2	0.5	5.8	1.0	9	2.6
A7/293	R	0.3	2.8	6.8	19	100	23	105	22	23	8	129	199	3.3	6.1	461	41	82	39	7.5	1.7	1.0	3.6	0.5	6.3	1.2	12	2.9
A7/294	R	0.3	2.6	6.7	18	96	14	108	20	17	14	125	206	3.5	5.3	433	41	83	38	7.0	1.6	0.9	3.3	0.5	6.2	1.1	11	2.7
A7/295	R	0.3	2.4	6.7	17	94	14	94	20	20	9	116	245	3.6	5.1	428	37	74	34	6.1	1.4	0.8	3.1	0.5	6.6	1.1	11	2.7
A9/190	R	0.3	2.9	6.6	17	98	12	88	24	30	8	130	230	3.3	5.4	433	43	83	37	7.3	1.6	1.0	3.2	0.5	6.9	1.2	11	2.7
A9/191	R	0.3	2.4	6.4	16	92	21	91	21	26	7	118	236	3.8	5.1	371	38	75	33	6.5	1.4	0.9	3.0	0.5	6.2	1.0	11	2.5
Cabeço dos Pendentes (CP)																												
A7/292	R	0.2	2.0	6.4	13	75	6	41	15	13	10	94	200	1.5	4.0	262	35	71	33	5.8	1.2	0.7	2.7	0.4	6.5	0.9	9	2.5
A9/192	R	0.2	2.7	5.0	15	84	6	51	21	11	22	124	200	1.5	5.1	385	36	70	33	6.7	1.3	0.9	2.8	0.5	6.1	1.0	10	2.8
Quinta do Paço II (QP)																												
A6/067	R	0.3	2.4	9.1	23	76	10	146	16	3	3	120	225	0.4	14	724	38	75	37	7.6	1.8	1.1	3.1	0.5	6.0	1.6	11	3.8
A6/068	R	0.2	2.1	12	25	122	10	140	19	25	3	109	241	0.0	16	719	43	68	41	8.1	2.0	1.1	3.1	0.5	5.7	2.1	10	3.3
A6/069	R	0.1	2.2	5.9	16	32	7	78	13	20	5	121	247	0.3	12	781	54	103	72	14	3.2	1.9	5.3	0.8	6.1	1.0	10	2.2
A6/070	R	0.2	2.3	5.2	14	26	7	96	12	8	2	107	225	0.2	12	682	28	66	28	6.5	1.4	0.8	2.6	0.4	6.7	0.9	9	2.2
A6/071	R	0.1	2.1	6.3	18	30	7	74	12	9	2	123	224	0.2	13	701	25	51	24	5.0	1.1	0.7	2.5	0.4	6.5	0.9	11	1.9
A6/072	R	0.1	1.9	5.7	16	29	5	78	10	7	1	99	188	0.2	12	667	26	89	32	6.7	1.6	0.9	3.3	0.6	5.7	0.9	13	2.2
A6/733	C	0.8	3.3	5.0	15	49	8	47	18	8	4	122	217	0.3	7.8	619	63	133	73	15	3.4	2.5	6.4	0.9	5.6	1.0	13	3.3
A6/734	C	1.0	4.0	6.6	16	87	9	56	23	12	15	133	176	0.6	11	714	39	70	35	6.9	1.4	1.0	3.2	0.5	4.7	1.1	11	2.8
A6/735	C	2.2	3.2	5.4	15	74	7	100	23	6	2	152	188	0.1	14	735	41	85	43	8.5	2.0	1.3	3.8	0.6	4.6	1.0	10	3.0
A6/736	C	0.3	3.8	6.0	28	145	30	79	43	28	28	109	481	0.8	14	531	44	89	47	11	2.6	1.4	4.9	0.8	13	2.1	20	5.6
Santa Margarida da Coutada (SMC)																												
A9/193	R	0.4	2.5	1.3	3	88	3	28	8	3	8	113	332	0.3	4.7	233	34	69	31	5.6	0.6	0.8	3.2	0.5	10	1.0	15	2.9
A9/194	R	0.3	2.8	1.1	3	17	3	24	8	3	4	115	286	0.0	4.5	237	37	75	33	6.3	0.6	0.7	2.2	0.3	8.9	1.1	17	3.0
A9/195	C	1.3	2.9	6.0	13	38	11	83	26	8	21	95	476	0.3	3.7	741	98	184	77	12	1.9	1.4	3.4	0.4	12	1.7	31	3.0
A9/196	C	1.7	2.8	5.9	17	100	10	78	25	8	7	131	205	0.2	8.2	491	34	67	32	5.9	1.1	0.9	2.9	0.4	5.4	1.0	11	3.4
Povoado de Fontes (FNT)																												
A9/202	R	0.2	0.8	2.2	5	35	4	36	11	9	26	43	191	0.6	3.1	122	21	43	18	3.7	0.7	0.4	1.4	0.2	5.6	0.9	8	2.1
A9/203	H	0.0	0.2	3.1	5	37	2	12	15	23	21	23	81	1.1	2.0	764	14	28	14	3.4	0.7	0.3	0.7	0.1	2.5	0.6	11	1.7
A9/204	H	0.0	0.3	2.6	4	34	2	12	16	22	14	27	90	1.0	2.5	735	11	22	11	2.7	0.5	0.2	0.7	0.1	2.6	0.6	10	1.7
A9/205	H	0.1	0.4	1.6	4	24	2	12	11	15	16	27	93	0.7	2.3	687	13	24	12	2.5	0.4	0.2	0.7	0.1	2.9	0.6	7	1.4
UCC		3.3	2.8	5.0	14	92	17	67	18	5	2	84	193	0.4	4.9	624	31	63	27	4.7	1.0	0.7	2.0	0.3	5.3	0.9	11	2.7
PAAS		1.2	3.7	7.2	16	110	23	85	20	–	–	160	210	–	15	650	38	80	32	5.6	1.1	0.8	2.8	0.4	5.0	–	15	3.0

**Table 7**

Summary interpretations of the luminescence dating results with respect to site chronologies and formation processes, and indications of their coincidence with regional archaeological and climatic patterns.

Reference (ITNLUM_)	Chronology	Interpretation		
		Event dated	Implications	Parallels
Anta da Lajinha (AL) 204 <sub>r1</sub> , 203 <sub>r1</sub> , 274, 205 <sub>r1</sub>	3200 BC–<1400 BC	Post construction pedoturbation/redeposition in surficial/peripheral locations.	Pedoturbation was effective in partially resetting OSL signals to c. 30 cm depth in mound	Peak in Megalithic and early Chalcolithic dates
206 <sub>r1</sub> , 438, 275, 202 <sub>r1</sub> , 273	4300 BC–3800 BC	Pedoturbation/accumulation shortly pre-construction. Usage/abandonment not detected	<i>Terminus post quem</i> : tumulus construction most likely circa 3800 BC, slightly post-dating the onset of Iberian Megalithic construction	Younger part of the main group of extant dates for Neolithic contexts. Increasing deforestation and arable production, drying climate
439	5200 BC–4600 BC	Accumulation/formation of colluvium/subsoil	Previous erosion to bedrock or intensive pedoturbation of thin regolith	Mesolithic–Neolithic transition, cool wet climate
Cabeço dos Pendentes (CP) 272	<1500AD	Effects of redeposition during early 20th century excavations	Chalcolithic site (re-)usage (abandonment or construction not precluded)	Oldest artefacts at CP; increasing anthropic impact; some extant dates from Megalithic contexts
440	2500 BC–1900 BC	Accumulation/emplacement of regolith in chamber with well reset OSL signals		
Quinta do Paço II (QP) 221, 223, 222	300 BC–1000 BC	Manufacture or use if for cooking	Phase of site usage mid-late Iron Age Pit closure probably end of the Iron Age	Fluctuating land-use intensity; followed by Romanization
220	1900 BC–1600 BC		Site usage in the Bronze Age: pits probably constructed in this period	Most extant dates from Bronze Age contexts, progressive deforestation
57 <sub>r1</sub> , 59 <sub>r1</sub>	1600 BC–1200 BC	Accumulation of regolith with well reset OSL signals from adjacent land surfaces.	Abandonment phase in the late Bronze Age: construction of pits prior to this	Follows a period of progressive deforestation
60 <sub>r1</sub>	>1400 BC–<150 BC	Pedoturbation of regolith/subsoil below land surfaces	Mixing of well reset regolith from the late Bronze Age with material from/in/until the late Iron Age	Apparently ceased/sealed around the beginning of the Roman period
56 <sub>r1</sub>	>6700 BC–<3500 BC		Mixing of regolith possibly reset in the early Holocene, with material from/in/until the late Neolithic	Clearance and establishment of agriculture in a drying climate
Santa Margarida da Coutada (SMC) 441	>2500 BC–<0 BC	Pedoturbation of sediments/colluviums derived from local Plio/Miocene clayey arenites: land surfaces with slight anthropic input	Accumulation in the Chalcolithic and Late Glacial (or earlier), pedoturbated until the Roman and Epipalaeolithic periods (or later). Lithics in the lower layer could relate to a range of periods	Warm, wet climate; fluctuating landscape pressure
442	>13500 BC–<7800 BC			Climate becoming warmer and wetter. Indications of clearance around the younger limit
443, 444	3900 BC–2900 BC	Manufacture or use if for cooking	Human presence in the mid Neolithic and Neolithic –Chalcolithic transition: long/repeated use or residuality/erosion	Climate wetter and landscape pressure significantly increased towards end of this period
Povoado de Fontes (FNT) 450	6100 BC–5300 BC	Slope wash/colluvial accumulation from mixed metamorphic and sedimentary sources	Cycles of local sedimentary erosion and redeposition, anthropogenic input	First main phase of agricultural activity in the region
452, 451, 453	8600 BC–8000 BC	Heating of <i>in situ</i> material by a fire-pit/oven during site occupation	Direct evidence for occupation in the late 9th millennium BC	Earliest indications of lowland clearance/cultivation. Dates for Epi- and Upper- Palaeolithic contexts

Results from sherds indicated broader and slightly different chronologies than synthetic typological designations for each assemblage: the late Neolithic was represented at SMC (early Chalcolithic, Cruz, 2006), and the Bronze Age and mid-late Iron Age at QP (late Chalcolithic – early Bronze Age, Caron et al., 2010), though this has been reinterpreted as consistent with the present results. Differences might relate to sampling: typological interpretation is necessarily based on diagnostic sherds, whereas provision of non-diagnostic sherds is preferred for destructive dating analysis. In the large negative features of QP the ceramics generally

give younger results than fills from the same feature, but come from slightly higher (Table 7; c.f. Barnett, 2000). Geochemical analysis of the fills from QP indicates they have suffered little anthropic influence including heating, and to be locally derived regolith. Overall the results indicate activity at QP from the mid 2nd to mid/late 1st millennium BC.

A group of consistent dating results with relatively low scatter in absorbed dose, from deep in the tumulus and fills at AL (ca. 4000 BC), appears to relate to resetting of the OSL signal during transport or pedoturbation of surficial material prior to

construction, and shortly post-dates indications of minor clearance activity in the regional pollen record (Table 1; Table 7). Younger than expected results from basal contexts at CP indicate that some of the material from around the periphery of the chamber was exposed to light during more recent disturbance (ITNLUM 272), but that the fill within the chamber may have originally accumulated during a Chalcolithic or Early Bronze Age phase of site use (2300 BC, ITNLUM 440).

Younger results from the vertical sequence of samples ITNLUM 202–4 at AL indicate pedoturbation to ca. 30 cm from the tumulus surface since its construction, similar to the findings of Bush and Feathers (2003). Similarly, some layers at QP and SMC may have underlain palaeo-land-surfaces until after the dates indicated by the younger end of the broad distributions of results from the multi-grain analyses used in the present study (ca. 150 BC, 3500 BC, 0 BC and 7800 BC for ITNLUM 60r1, 56r1, 441, and 442 respectively; Fig. 3; Table 7).

Little scatter and a younger result (5700 BC) than from the structure it sealed and surrounded (8300 BC) indicates that the regolith sample from FNT represents sedimentary accumulation following erosion, and also that it has not been affected by pedoturbation, so until recently it was probably buried deeper than when sampled (Table 7). The structure at FNT represented a context in its own right. Comparison of OSL and TSL results confirmed it was heated, and its mineralogical and geochemical similarity to the more recent sediment surrounding it indicates that it is the base of a fire pit cut into a lost land surface. The date estimate for the structure is coincident with a broad maximum in *Quercus*, a local minimum in *Pinus*, a peak in *Poaceae*, and the first appearance of *Cerialia*-type pollen in the regional record (van der Knaap and van Leeuwen, 1995), and the beginning of a period of increased charred particle accumulation (Connor et al., 2012). Establishment of the diachronic distribution of such structures may help indicate the relative importance of anthropogenic environmental influences on this landscape in the early Holocene.

## 6. Conclusions

The 28 regolith and ceramic samples, from passage tombs, pit fills, a stone-scatter structure, and a fire pit/oven, associated with the transition to and development of agricultural societies in the Alto Ribatejo, produced OSL dates from throughout Holocene pre-history. They indicate occupation of the Alto Ribatejo landscape around the time of the first indications of clearance in the regional pollen record (FNT; late 9th millennium BC), but no signs of landscape activation (SMC) until the first indications of agriculture (FNT, erosion at AL also possibly at this time). Sediment accumulation/soil formation was observed around the transition to the Neolithic (FNT, AL; 5/6th millennium BC), but no direct evidence of early Neolithic occupation or megalithic construction was obtained. Clearance episodes were not directly identified in present samples, although a possible relationship to small scale regional indications was observed at AL (late 5th millennium BC), where local data indicate that significant vegetation coverage may not have existed in the time-frame of interest. Occupation at two sites began in the mid to late Neolithic (AL, SMC; early 4th millennium BC) and was accompanied by variable indications of landscape pressure (AL, SMC, QP). Occupation and landscape activation at four sites was observed in the Chalcolithic/Early Bronze Age (AL, CP, SMC, FNT; 3rd millennium BC), coincident with regional signals. The study sites contained records of occupation and variable landscape pressure in the Bronze and Iron Ages, which ceased with the Roman conquest (SMC, FNT, QP).

The present results illustrate how the combination of OSL dating of sediments and ceramics with geochemical and mineralogical

analysis is a powerful tool for understanding complex site formation processes on a site-by-site basis. The combination of OSL, INAA, FGS, HRGS, and XRD, is effective for understanding both dosimetric and luminescence behaviour, and so for investigating site formation processes. This produces a rather complex matrix of information for analysis, but comparison of indications and counter-indications from different sources allows a more secure interpretational framework to be constructed.

With respect to sampling of regolith, analysis of samples from the geological substrate and the present surface in addition to the archaeological contexts would aid the interpretation of results. When dating tumuli, samples from near the bottom are most useful unless post-depositional effects are of interest. For ceramic samples, analysis of diagnostic as well as undiagnostic sherds is important to avoid bias and facilitate comparison with typological interpretations. Overall, analysis of a variety of sample types is important to identify all relevant chronological phases. Fire pits or other heated structures appear ideal to map early landscape usage in the Alto Ribatejo, subject to careful radiometric and geochemical characterization.

## Acknowledgements

This work was funded by the FCT project PTDC/HAH/71361/2006. Implementation of gamma spectrometry and environmental dosimetry evaluation was supported by the grants REEQ/590/CTE/2005 and PTDC/AAC-AMB/121375/2010. Excavations at AL and CP were funded by British Academy Larger Research Grant LRG–42469 “Megalithic monuments and landscapes of the Upper Tagus Valley, Portugal”.

Editorial handling by: F. Preusser

## References

- Abrañes, F., Lebreiro, S., Rodrigues, T., Gil, I., Jonsdottir, H., Oliveira, P., Kissel, C., Grimalt, J.O., 2005. Shallow marine sediment cores record climate variability and earthquake activity off Lisbon (Portugal) for the last 2000 years. *Quat. Sci. Rev.* 24, 2477–2494.
- Adamiec, G., Aitken, M.J., 1998. Dose-rate conversion factors: update. *Ancient TL* 16, 37–49.
- Aitken, M.J., 1985. *Thermoluminescence Dating*. Academic Press, London.
- Anders, E., Grevesse, N., 1989. Abundances of the elements: meteoritic and solar. *Geochem. Cosmochem. Acta* 53, 197–214.
- Barnett, S.M., 2000. Sampling pottery in luminescence dating studies. *Radiat. Meas.* 32, 467–472.
- Batista, A., 2004. *Carta Arqueológica do Concelho de Constância*. Câmara Municipal de Constância, Constância.
- Bell, W.T., 1979. Attenuation factors for the absorbed radiation dose in quartz inclusions for thermoluminescence dating. *Ancient TL* 8, 2–13.
- Bell, W.T., Zimmerman, D.W., 1978. Effect of HF acid etching on morphology of quartz inclusions for thermoluminescence dating. *Archaeometry* 20, 63–65.
- Burbidge, C.I., 2003. *Luminescence Investigations and Dating of Anthropogenic Palaeosols from South Mainland Shetland*. University of Wales, Aberystwyth, p. 396 (Unpublished PhD thesis).
- Burbidge, C.I., Sanderson, D.C.W., Housley, R.A., Allsworth Jones, P., 2007. Survey of Palaeolithic sites by luminescence profiling, a case study from Eastern Europe. *Quat. Geochronol.* 2, 296–302.
- Burbidge, C.I., Dias, M.I., Prudêncio, M.I., Rebêlo, L.P., Cardoso, G.O., Brito, P., 2009. Internal  $\alpha$  activity: localisation, compositional associations and effects on OSL signals in quartz approaching  $\beta$  saturation. *Radiat. Meas.* 44, 494–500.
- Bush, D.A., Feathers, J.K., 2003. Application of OSL single-aliquot and single-grain dating to quartz from anthropogenic soil profiles in the SE United States. *Quat. Sci. Rev.* 22, 1153–1159.
- Cardoso, G., Oosterbeek, L., Dias, M.I., 2012. Construção de uma base de dados de datações de sítios arqueológicos da Península Ibérica: contribuição para o estudo de sequências cronológicas. *Estudos Arqueológicos de Oeiras* 19, 305–310.
- Caron, L., Freitas, A., Oosterbeek, L., 2010. Variante à E. N. 238 entre a E. N. 110 (IC3) e proximidades de Ferreira do Zêzere. In: *Intervenções Arqueológicas Efectuadas pelo CEIPHAR, Acompanhamento e Sondagens realizadas em contexto de obra. Estradas de Portugal, S.A.*, pp. 8–9. <http://www.estradasdeportugal.pt/index.php/pt/areas-de-actuacao/gabinete-de-ambiente/481-revista-digital-de-arqueologia>.

- Carvalho, A.F., 2010. Chronology and geography of the Mesolithic-Neolithic transition in Portugal. In: Armbruster, T., Hegewisch, M. (Eds.), *On Pre- and Earlier History of Iberia and Central Europe. Studies in Honour of Philine Kalb*. Habelt-Verlag, Bonn, pp. 15–61. <http://ualg.academia.edu>.
- Chaminé, H.I., Gama Pereira, L.C., Fonseca, P.E., Noronha, F., Lemos de Sousa, M.J., 2003. Tectonoestratigrafia da faixa de cisalhamento de Porto-Albergaria-a-Velha-Coimbra-Tomar, entre as Zonas Centro-Ibérica e de Ossa-Morena (Maciço Ibérico, W de Portugal). *Cadernos Lab*, vol. 28, pp. 37–78. Xeolóxico de Laxe, Coruña.
- Connor, S.E., Araújo, J., van der Knaap, W.O., van Leeuwen, J.F.N., 2012. A long-term perspective on biomass burning in the Serra da Estrela, Portugal. *Quat. Sci. Rev.* 55, 114–124.
- Cruz, A., 2006. Santa Margarida da Coutada (Constância) Campanha Arqueológica – 2006. Notícia Preliminar sobre a Intervenção no Povoado de Santa Margarida da Coutada. Centro de Pré-História do Instituto Politécnico de Tomar. <http://www.cph.ipt.pt/angulo2006/img/06-07/SMAC.pdf>.
- Cruz, A., 2007. A Pedra da Encavalada. In: *Angulo, Serie I*, pp. 1–16 (2006/07) [http://www.cph.ipt.pt/angulo/index.php?option=com\\_jotloader&section=files&task=download&cid=64\\_6ce8c2c286d5fa98cd7e28e8d040ad9e&Itemid=14](http://www.cph.ipt.pt/angulo/index.php?option=com_jotloader&section=files&task=download&cid=64_6ce8c2c286d5fa98cd7e28e8d040ad9e&Itemid=14).
- Cruz, A., 2010. Relatório da Campanha de Escavação de Fontes – 2010 (Povoado de Fontes). Centro de Pré-História do Instituto Politécnico de Tomar. [http://www.cph.ipt.pt/angulo/index.php?option=com\\_jotloader&view=categories&cid=13\\_c0bcad828bb9c3077c660d2aac7b3380&Itemid=18](http://www.cph.ipt.pt/angulo/index.php?option=com_jotloader&view=categories&cid=13_c0bcad828bb9c3077c660d2aac7b3380&Itemid=18).
- da Silva, L.H., 1939. Monografia de Cardigos. Cucujães: Escola Tipica das Missões.
- Deckers, K., Sanderson, D.C.W., Spencer, J.Q., 2005. Thermoluminescence screening of non-diagnostic sherds from stream sediments to obtain a preliminary alluvial chronology: an example from Cyprus. *Geoarchaeology* 20, 67–77.
- Dias, M.I., Prudêncio, M.I., 2007. Neutron activation analysis of archaeological materials: an overview of the ITN NAA Laboratory, Portugal. *Archaeometry* 49, 383–393.
- Dias, M.I., Prudêncio, M.I., 2008. On the importance of using scandium to normalize geochemical data preceding multivariate analyses applied to archaeometric pottery studies. *Microchem. J.* 88, 136–141.
- Duller, G.A.T., 2003. Distinguishing quartz and feldspar in single grain luminescence measurements. *Radiat. Meas.* 37, 161–165.
- Figueiredo, A., 2007. Entre as Grutas e os Monumentos Megalíticos: problemáticas e interrogações na Pré-História recente do Alto Ribatejo. *Al-madan Online* 15, 1–15.
- Fleming, S.J., 1970. Thermoluminescence dating: refinement of the quartz inclusion method. *Archaeometry* 12, 133–145.
- Galbraith, R.F., Roberts, R.G., Laslett, G.M., Yoshida, H., Olley, J.M., 1999. Optical dating of single and multiple grains of quartz from jinnium rock shelter, northern Australia, part 1, Experimental design and statistical models. *Archaeometry* 41, 339–364.
- Gouveia, M.A., Prudêncio, M.I., 2000. New data on sixteen reference materials obtained by INAA. *J. Radioanal. Nucl. Chem.* 245, 105–108.
- Govindaraju, K., 1994. Compilation of working values and sample description for 383 geostandards. *Geostandards Newsl.* 18.
- Guibert, P., Lahaye, C., Bechtel, F., 2009. The importance of U-series disequilibrium of sediments in luminescence dating: a case study at the Roc de Marsal Cave (Dordogne, France). *Radiat. Meas.* 44, 223–231.
- Krane, S.K., 1988. *Introductory Nuclear Physics*. Wiley.
- LNEG 2013. <http://geoportal.lneg.pt/geoportal/mapas/index.html>. 24/01/2013.
- Martini, M., Spinolo, G., Vedda, A., 1987. Defects dynamics in as-grown and electrodiffused quartz: and interpretation of the predose effect. *J. Appl. Phys.* 61, 2486–2488.
- Mejdahl, V., 1979. Thermoluminescence dating: beta-dose attenuation in quartz grains. *Archaeometry* 21, 61–72.
- Mejdahl, V., 1983. Feldspar inclusion dating of ceramics and burnt stones. *Counc. Europe PACT J.* 9, 351–364.
- Murphy, P.J., Roberts, S., 1997. Evolution of a metamorphic fluid and its role in lode gold mineralisation in the Central Iberian Zone. *Mineralium Deposita* 32, 459–474.
- Murray, A.S., Wintle, A.G., 2000. Luminescence dating of quartz using an improved single-aliquot regenerative-dose protocol. *Radiat. Meas.* 32, 57–73.
- NIST ESTAR. 2009. <http://physics.nist.gov/PhysRefData/Star/Text/ESTAR.html>. 15/06/2009.
- Oliveira, J.T., Pereira, E., Ramalho, M., Antunes, M.T., Monteiro, J.H., 1992. Carta Geológica de Portugal à escala 1:500000, 5ª edição. Serviços Geológicos de Portugal, Lisboa.
- Oosterbeek, L., 2001. Re-thinking the Mesolithic-Neolithic transition in the Iberian Peninsula: a view from the West. In: *Documenta Praehistorica XXVIII. Neolithic Studies*, vol. 8, pp. 75–84.
- Ortega, L., Oyarzun, R., Gallego, M., 1996. The Mari Rosa late Hercynian Sb-Au deposit, western Spain. *Geology and geochemistry of the mineralizing processes. Mineralium Deposita* 31, 172–187.
- Pais, J., Cunha, P., Pereira, D., Legoinha, P., Dias, R., Moura, D., Silveira, A., Kullberg, J., Gonzales-Delgado, J.A., 2012. The Paleogene and Neogene of Western Iberia (Portugal). *Springer Briefs in Earth Sciences*, Springer, Heidelberg.
- Prescott, J.R., Hutton, J.T., 1988. Cosmic-ray and gamma-ray dosimetry for TL and Electron-Spin- resonance. *Nucl. Tracks Radiat. Meas.* 14, 223–227.
- Prescott, J.R., Stephan, L.G., 1982. The contribution of cosmic radiation to the environmental dose for thermoluminescent dating. *Latitude, altitude and depth dependencies. Counc. Europe PACT J.* 6, 17–25.
- Prudêncio, M.I., Braga, M.A.S., Oliveira, F., Dias, M.I., Delgado, M., Martins, M., 2006. Raw material sources for the roman bracarense ceramics (NW Iberian Peninsula). *Clays Clay Miner.* 54, 638–649.
- Reimer, P.J., Baillie, M.G.L., Bard, E., Bayliss, A., Beck, J.W., Blackwell, P.G., Bronk Ramsey, C., Buck, C.E., Burr, G., Edwards, R.L., Friedrich, M., Grootes, P.M., Guilderson, T.P., Hajdas, I., Heaton, T.J., Hogg, A.G., Hughen, K.A., Kaiser, K.F., Kromer, B., McCormac, F.G., Manning, S.W., Reimer, R.W., Richards, D.A., Southon, J., Turney, C.S.M., van der Plicht, J., Weyhenmeyer, C., 2009. IntCal09 and Marine09 radiocarbon age calibration curves, 0–50,000 years cal BP. *Radiocarbon* 51, 1111–1150.
- Ribeiro, O., Teixeira, C., Gonçalves, F., Zbyszewski, G., 1977. Carta Geológica de Portugal à escala 1:50000, 27–D (Abrantes). Serviços Geológicos de Portugal, Lisboa.
- Richter, D., Zink, A., Przegietka, K., Cardoso, G.O., Gouveia, M.A., Prudêncio, M.I., 2003. Source calibrations and blind test results from the new Luminescence Dating Laboratory at the Instituto Tecnológico e Nuclear, Sacavém, Portugal. *Ancient TL* 21, 1–7.
- Roberts, H.M., Duller, G.A.T., 2004. Standardised growth curves for optical dating of sediment using multiple grain aliquots. *Radiat. Meas.* 38, 241–252.
- Rowell, D.L., 1994. *Soil Science: Methods and Applications*. Longman, Harlow.
- Rowley-Conwy, P., 2011. Westward Ho! The spread of agriculturalism from central Europe to the Atlantic. *Curr. Anthropol.* 52, S431–S451.
- Rubel, F., Kottek, M., 2010. Observed and projected climate shifts 1901–2100 depicted by world maps of the Köppen-Geiger climate classification. *Meteorologische Z.* 19, 135–141.
- Rudnick, R.L., Gao, S., 2003. Composition of the continental crust. In: Holland, H.D., Turekian, K.K. (Eds.), *Treatise on Geochemistry: the Crust*. Elsevier, pp. 1–64.
- Scarre, C., 2007. Changing places: monuments and the neolithic tradition in western France. *Proc. Br. Acad.* 144, 243–261.
- Scarre, C., Oosterbeek, L., 2010. The megalithic tombs of the middle Tagus basin and agro-pastoral origins in Western Iberia. In: Armbruster, T., Hegewisch, M. (Eds.), *Beiträge zur Vor- und Frühgeschichte der Iberischen Halbinsel und Mitteleuropas. Studien in honorem Philine Kalb*. Habelt, Bonn, pp. 97–110.
- Scarre, C., Arias, P., Burenhult, G., Fano, M.A., Oosterbeek, L., Schulting, R.J., Sheridan, A., Whittle, A., 2003. Megalithic chronologies. In: *Stones and Bones. Formal Disposal of the Dead in Atlantic Europe during the Mesolithic-neolithic Interface 6000–3000 BC*. Archaeopress, Oxford, pp. 65–111.
- Scarre, C., Oosterbeek, L., French, C., 2011. Tombs, landscapes and settlement in the Tagus hill-country. In: Bueno Ramirez, P., Cerrillo Cuenca, E., Gonzalez Cordero, A. (Eds.), *From the Origins: the Prehistory of the Inner Tagus Region*. Archaeopress, Oxford, pp. 83–91.
- Stabin, M.G., da Luz, L.C.Q.P., 2002. Decay data for internal and external dose assessment. *Health Phys.* 83, 471–475.
- Taylor, S.R., McLennan, S.M., 1985. *The Continental Crust: Its Composition and Evolution*. Blackwell Scientific Publications, Oxford, UK.
- Trindade, M.J., Dias, M.I., Rocha, F., Prudêncio, M.I., Coroado, J., 2011. Bromine volatilization during firing of calcareous and non-calcareous clays: archaeometric implications. *Appl. Clay Sci.* 53, 489–499.
- Trindade, M.J., Prudêncio, M.I., Burbidge, C.I., Dias, M.I., Cardoso, G., Marques, R., Rocha, F., 2013. Distribution of naturally occurring radionuclides (K, Th and U) in weathered rocks of various lithological types from the uranium bearing region of Fornos de Algodres, Portugal. *Mediterr. Archaeology Archaeometry* 13 (3) (in press).
- van der Knaap, W.O., van Leeuwen, J.F.N., 1995. Holocene vegetation succession and degradation as responses to climatic change and human activity in the Serra da Estrela, Portugal. *Rev. Palaeobot. Palynol.* 89, 153–211.
- van der Schriek, T., 2004. *Holocene Environmental Change and the Alluvial Geoarchaeology of Mesolithic Settlement-subsistence in the Muge and Magos Valleys, Lower Tagus Basin, Portugal*. Unpublished Ph.D. thesis. University of Newcastle upon Tyne, England.
- Villaseca, C., Bellido, F., Perez-Soba, C., Billstrom, K., 2009. Multiple crustal sources for post-tectonic I-type granites in the Hercynian Iberian Belt. *Mineral. Petrol.* 96, 197–211.
- Vis, G.-J., Bohncke, S.J.P., Schneider, H., Kasse, C., Coenraads-Nederveen, S., Zuurbier, K., Rozema, J., 2010. Holocene flooding history of the Lower Tagus Valley (Portugal). *J. Quat. Sci.* 25, 1222–1238.
- White, A.F., 2008. Chapter 10, quantitative approaches to characterizing natural chemical weathering rates. In: Brantley, S., Kubicki, J., White, A. (Eds.), *Kinetics of Water-rock Interaction*. Springer Science+Business Media, LLC, pp. 469–543. Ch 10.
- Whittle, E.H., Arnaud, J.M., 1975. Thermoluminescent dating of Neolithic and Chalcolithic pottery from sites in central Portugal. *Archaeometry* 17, 5–24.
- Zacharias, N., Schwedt, A., Buxeda i Garrigo's, J., Michael, C.T., Mommsen, H., Kilikoglou, V., 2007. A contribution to the study of post-depositional alterations of pottery using TL dating analysis. *J. Archaeol. Sci.* 34, 1804–1809.
- Zapata, L., Peña-Chocarro, L., Pérez-Jordá, G., Stika, H.-P., 2004. Early Neolithic agriculture in the Iberian Peninsula. *J. World Prehistory* 18, 283–325.
- Zilhão, J., 1997. Maritime pioneer colonisation in the early Neolithic of west Mediterranean. Testing the model against evidence. *Porçilo O Raziskovanju Paleolitika, Neolitika in Eneolitika v Sloveniji* 24, 19–24.
- Zimmerman, D.W., 1971. Thermoluminescence dating using fine grains from pottery. *Archaeometry* 13, 29–52.